SADI International Journal of Science, Engineering and Technology
ISSN: 2837-1941| Impact Factor: 8.27
Volume. 12, Number 4; October-December, 2025;
Published By: Scientific and Academic Development Institute (SADI)
8933 Willis Ave Los Angeles, California
https://sadijournals.org/index.php/sijset|editorial@sadijournals.org

SYNCHRONOUS GENERATOR TERMINAL VOLTAGE REGULATION UNDER DYNAMIC LOAD CONDITIONS USING MODEL-FREE ADAPTIVE CONTROL AND H-INFINITY CONTROLLER

[1]David Oluwagbemiga Aborisade, [2]Johnson Opeyemi Abiola and [1]Muniru Olajide Okelola
[1]Department of Electronic and Electrical Engineering, Ladoke Akintola University of Technology, Ogbommoso, Oyo State, Nigeria
[2*]Department of Mechatronics Engineering, Bells University of Technology, Ota, Ogun State, Nigeria
Email: abiola.johnson@outlook.com **(0009-0005-1081-1768)**

ABSTRACT: This study compares the performance of the model-free adaptive control (MFAC) and H-infinity control strategies for terminal voltage control of synchronous generators under dynamic load conditions. The AVR system, incorporating a lead-lag compensator as a stabilizer, was tested under no-load, 20%, 50%, and 80% load scenarios using MATLAB/Simulink simulations. The results demonstrate that MFAC offers faster response times (0.36 s rise time at no-load) compared to the H-infinity controller (1.56 s) and exhibits significantly higher overshoot (40.14%) compared to the H-infinity controller (17.15%). The H-infinity controller provides superior stability with minimal overshoot and robust performance across all load conditions. Therefore, the H-infinity controller emerges as the optimal solution for power systems requiring precise voltage regulation under varying loads, particularly in unstable grids such as Nigeria's.

Keywords: H-infinity, model-free adaptive control, terminal voltage regulation, synchronous generator, automatic voltage regulator

1. INTRODUCTION

The global demand for a stable and reliable supply of electricity is increasing, emphasizing the crucial role of effective control techniques in power systems [1]. The synchronous generator, which is a critical component responsible for converting mechanical energy into electrical energy, lies at the heart of electricity generation [2]. The automatic voltage regulator (AVR) plays a critical role in maintaining a steady terminal voltage to ensure the easy integration of this power into the power grid, even in the face of load and external disturbances [3].

Power system stability is greatly dependent on the effective regulation of terminal voltage, and the AVR becomes a central component in synchronous generator operations [1]. The frequency and power composition in various realms of power system operations are influenced by the load variations and faulty conditions [4]. One of the main issues in the management of power systems is maintaining the stability and consistency of the standard voltage level so that all the related equipment is designed for the same pre-established voltage level [5]. Since the

terminal voltage of the synchronous generator (SG) is affected by unavoidable variations in load demands, a control system that can react to such changes [6] while maintaining voltage stability is important [7]. An automatic voltage regulator (AVR) is intended to regulate the excitation of synchronous generators in such a way that a steady terminal voltage is preserved [1]. However, the inherent high inductance of synchronous generator field windings coupled with load variations makes it difficult for the AVR to provide a steady and quick response. The addition of a Lead-lag feedback compensator is of paramount importance. This compensator improves the stability of the AVR by improving the dynamic response characteristics of the system [1]. Although stability enhancement has improved, the intrinsic dynamic nature of power systems demands adaptive control methods that can effectively handle generator characteristic changes [8].

An appropriate controller is necessary to enhance the dynamic performance of the automatic voltage regulator (AVR); however, the choice of an appropriate controller is one of the most challenging parts in AVR system development [9]. Various controllers have been developed and optimized to enhance the performance of the synchronous generator automatic voltage regulator (AVR), i.e., proportional integral derivative (PID) and linear quadratic Gaussian (LQG), among others; however, they have all demonstrated limitations in terms of accuracy in response time when there are changing load conditions [10]. A more dynamic voltage-controlling mechanism is crucial for improving the performance of an SG AVR system.

MFAC techniques is a viable way of withstanding uncertainty and changing operating condition parameters. Integration of MFAC into an AVR adds a vital element of adaptability, which remains crucial for real-time feedback against generator parameter changes. Compared with traditional control systems based on preestablished models, MFAC has a tendency to adjust automatically to the changing characteristics of the generator and thus maximizes performance under a wide variety of operating conditions [11].

Additionally, the H-infinity controller is another method implemented in the system to implement the optimal control policy, chosen based on its suitability in handling disturbances and uncertainties. The controller reduces the impact of disturbances by reducing a certain performance measure, thus offering stable and optimal control when there is uncertainty [12].

To confirm the effectiveness of the proposed control methods, the simulations were conducted using MATLAB/SIMULINK version 2023b. The model used in the simulation includes mathematical modeling of the AVR system, the lead-lag controller, and the other two controllers. Simulation enables a thorough examination of the system's response under various loads, thus reflecting its dynamic performance and behavioral characteristics [13]. The system performance was investigated by examining aspects such as peak time, rise time, settling time, and percentage overshoot.

Several researchers have contributed to the control approaches for SG terminal voltage regulation, some of them are as in Table 1, which covered works from 2014 to 2024.

Table 1. Key Findings

Authors	Controller Type	Optimization algorithm (OA)	Key Contribution	Limitation

[14]	PID, IC, and FOPID	Various group with OA such as PSO, GA, GWO, and ABC)	Comprehensive review of group with OA for optimizing AVR controller parameters (PID, IC, and FOPID) to improve stability and time-domain response (OS, RT, ST, and SSE).	Focuses on controller optimization
[15]	FOPIDD² (Novel)	Reptile search algorithm (RSA)	Proposed novel FOPIDD² controller tuned by RSA outperformed 22 recent studies. Improved transient response.	We did not examine load changes or disturbances.
[16]	LQGTC	LQG	LQG-tuned controller (LQGTC) was used to reduce oscillations and guarantee stable performance across various parameters.	Did not account for load variations or external disturbances.
[17]	PID	PSO, CS	Optimized PID gains using PSO and CS with a novel objective function (IAE, RT, ST, and OS). CS achieved the best time-domain performance.	Did not account for load changes or perturbations.
[18]	PID, FOPID, PIDD²	SA-MRFO (Hybrid)	Proposed hybrid simulated annealing-manta-ray foraging optimization (SA-MRFO) for PID parameterization. PIDD² showed the largest improvement (79% faster RT/ST, 58% lower OS vs. conventional PID).	Focuses on the optimization method.
[19]	PID	Symbiotic Organism Search	Optimized PID with SOS using an enhanced cost function Improved stability and robustness to parameter variations and external disturbances.	The increased third weighting factor degraded the rise and settling times.
[20]	PID	N/A	Improved digital excitation control system (DECS) performance, reducing overshoot from 75% to 16%.	Focuses on the DECS problem.
[21]	PIDD + Prefilter (Novel)	N/A	Proposed PIDD with a prefilter to address large overshoot from PIDD alone. The pre-filter setup provided optimal performance (fast response, minimum overshoot).	Performance was not verified under actual load changes or disturbances.

[22]	PID, Cascade, and IMC	N/A	Comparative study: IMC provided optimal stability (0% overshoot) but was slower than other methods. The cascade was well balanced. PID was the fastest but had a high overshoot.	We did not examine performance under load variation.

While numerous studies focus on optimizing controller parameters (PID, FOPID, PIDD², etc.) to enhance AVR performance, a common limitation is the failure to address performance under varying loading conditions and external disturbances. Conventional PID controllers struggle to maintain optimal performance under these real-world conditions. Only [19] and [22] explicitly tested robustness, with [19] showing success but a trade-off in response speed, and [22] noting the lack of load variation testing and external disturbance as a research gap. The trend shows a shift toward adaptive (H-infinity) and robust (MFAC) control strategies capable of maintaining voltage stability under varying loads and disturbances.

2. MATERIALS AND METHODS

2.1 Automatic Voltage Regulator

Figure 1 shows a typical AVR system of a synchronous generator. Four essential components constitute an AVR system: amplifier, exciter, generator, and the output voltage measurement sensor [23].

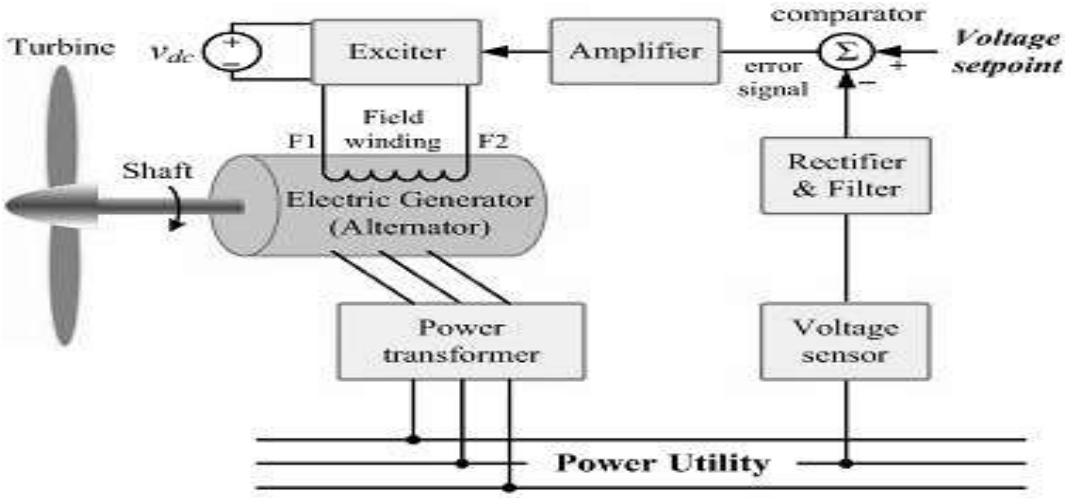

Figure 1. Schematic of an AVR of a Synchronous Generator [19]

A. Amplifier model

The amplifier is a model first-order differential system with a time constant T_a and gainK_a. According to [21], the differential equation representing the relationship between the output voltage $V_R(t)$ and the input voltage $V_e(t)$ of the amplifier according to [21] is given as equation (1).

$$V_R(t) + T_a \frac{dV_R(t)}{dt} = K_a V_e(t) \quad 1$$

This differential equation is converted into the frequency domain using the Laplace transform, and let $G_a(s)$ be the ratio of the output voltage $V_R(s)$ to the input voltage$V_e(s)$, then the amplifier model is given by equation (2).

$$G_a(s) = \frac{K_a}{1+sT_a} \quad 2$$

Where, K_a is the amplifier gain and T_a is the time constant of the amplifier. K_a Has a typical value ranging from 10 to 40, and the time constant is negligible but ranges from 0.02 to 0.1 s.

B. Exciter model

Modern generator exciters use an AC power source through solid-state rectifiers [24]. The exciter's output voltage is usually a nonlinear function of the generator field voltage because of the usual magnetic circuit. This implies that there is no simple relationship between the exciter's terminal voltage and field voltage [25]. The IEEE committee on excitation system recommended a reasonable linearized model that includes most of the time constants and ignores the saturation and nonlinearity effect. A time constant T_e and gain K_e is used in the transfer function of the exciter [26]. According to [21], the differential equation representing the relationship between the output voltage $V_f(t)$and the input voltage $V_R(t)$ of the exciter according to [21] is given as equation (3).

$$V_f(t) + T_e \frac{dV_f(t)}{dt} = K_e V_R(t) \quad 3$$

Equation (2.3) is converted into the frequency domain using the Laplace transform, and let $G_e(s)$ be the ratio of the output voltage $V_f(s)$ to the input voltage $V_R(s)$, then the exciter model is given by Equation (4):

$$G_e(s) = \frac{K_e}{1+sT_e} \quad 4$$

Where:

K_e is the exciter gain and

T_e is the exciter time constant.

The typical values of K_e and T_e are in the range of 1.0–10 and 0.4–1.0 s, respectively.

C. Generator model

The generated e.m.f. of the synchronous machine is usually a function of the machine magnetization curve, and its terminal voltage depends on the generator [27]. According to [28], the differential equation representing the relationship between the generator output voltage $V_t(t)$ and the field voltage $V_f(t)$ for the generator according to [28] is given as equation (5).

$$V_t(t) + T_g \frac{dV_t(t)}{dt} = K_g V_f(t) \quad 5$$

By converting this differential equation into the frequency domain using Laplace transform, and let $G_a(s)$ be the ratio of the output voltage $V_t(s)$ to the input voltage$V_f(s)$, then the amplifier model is given by the equation (6).

$$G_g(s) = \frac{K_g}{1+sT_g} \quad 6$$

The typical values of the gain and time constant are in the range of 0.7–1.0 and 1.0–2.0 s, respectively, from full load to no load. However, in this study, the internal dynamic of the generator is neglected to consider the external load, and it is assumed that $K_g = 1.0$ and $T_g = 0$ for the generator to respond instantaneously to changes in the field volatage with no time delay.

D. Sensor model

The voltage is sensed through a potential transformer and rectified through a bridge rectifier. According to [28], the differential equation representing the relationship between the sensor output voltage $V_s(t)$ and the generator terminal voltage $V_t(t)$ for the sensor according to [28] is given as equation (7).

$$V_s(t) + T_s \frac{dV_s(t)}{dt} = K_s V_t(t) \quad 7$$

The differential equation is converted into the frequency domain using the Laplace transform, and let $G_s(s)$ be the ratio of the output voltage $V_s(s)$ to the input voltage$V_t(s)$, then the amplifier model is given by Eq. (8).

$$G_s(s) = \frac{K_s}{1+sT_s} \quad 8$$

Where, K_{sen} is the sensor gain and T_{sen} is the time constant of the sensor. The typical values are in the range of 1.0–2.0 and 0.001–0.006 s.

Therefore, by combining all the models' transfer functions in Equations (2), (4), (6), and (8), and finding the closed-loop equation, we obtain Equation (9) which is the transfer function of the AVR system of a synchronous generator shown in Figure 2.

$$\frac{\Delta V_t(s)}{\Delta V_{ref}(s)} = \frac{K_a K_e K_g (1+sT_s)}{(1+sT_a)(1+sT_e)(1+sT_g)(1+sT_s)+K_a K_e K_g K_s} \quad 9$$

The generator's terminal voltage $Vt(s)$ is constantly detected by the sensor and then compared with the reference voltage$Vref(s)$. The distinction between the reference and the sensed terminal voltage (called error voltage) is amplified by the amplifier and used up by the exciter to excite the generator [29].

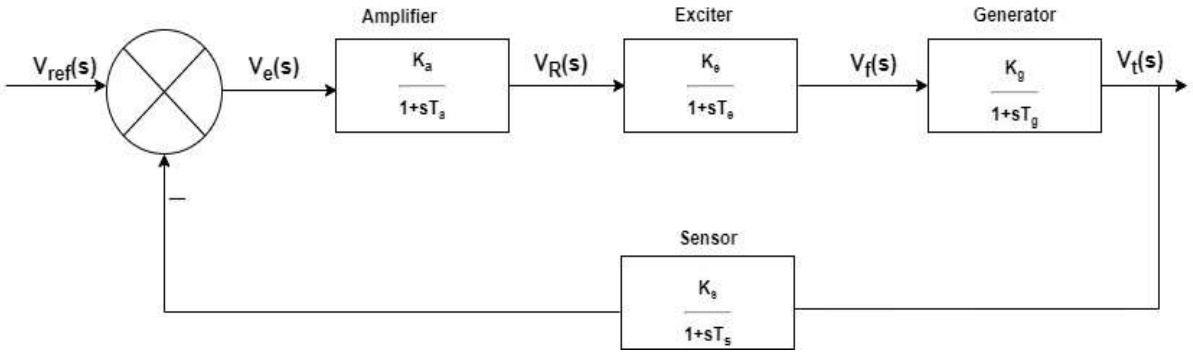

Figure 2. Automatic voltage regulator block diagram

2.2 Modeling of the Compensated AVR Model with Load

The preliminary findings in the literature show that the steady-state error of a typical AVR system is always high, which can also lead to a higher steady-state error, especially the overshoot and taking longer time to settle. Therefore, to reduce this error, the amplifier gain must be increased. However, this increment in the amplifier gain can also make the system unstable due to the arbitrary nature of selecting the value [30]. Therefore, a lead-lag compensator [31] is introduced as feedback to the AVR in Figure 2 between the input $V_e(s)$ and the output $V_f(s)$ of the block diagram to stabilize the system, as shown in Figure 3. The Lead-lag compensator is mathematically represented as equation (10).

$$G_n(s) = \frac{1+s(\alpha T_{n_1})}{1+sT_{n_2}} \quad 10$$

where, G_n is the Lead-lag transfer function, T_{n_1} is the lead time constant, T_{n_2} is the lag time constant, and α is the scaling factor.

Since the dynamic load is considered in this article, the generator G_g internal dynamic is ignored and considered as an ideal voltage source with no internal dynamic. The load G_L connected to the generator terminals introduces dynamic variations (sudden change) in the system that influence the terminal voltage based on the time it stays connected to the system. The load will be model as first order dynamic load (time-dependent), given as Equation (11).

$$G_L(s) = \frac{K_L}{1+sT_L} \quad 11$$

where, K_L is the proportional effect of the load on the terminal voltage typically between 0.5 and 1.0, T_L is the time taken for the load to impact the terminal voltage, and G_L is the load response.

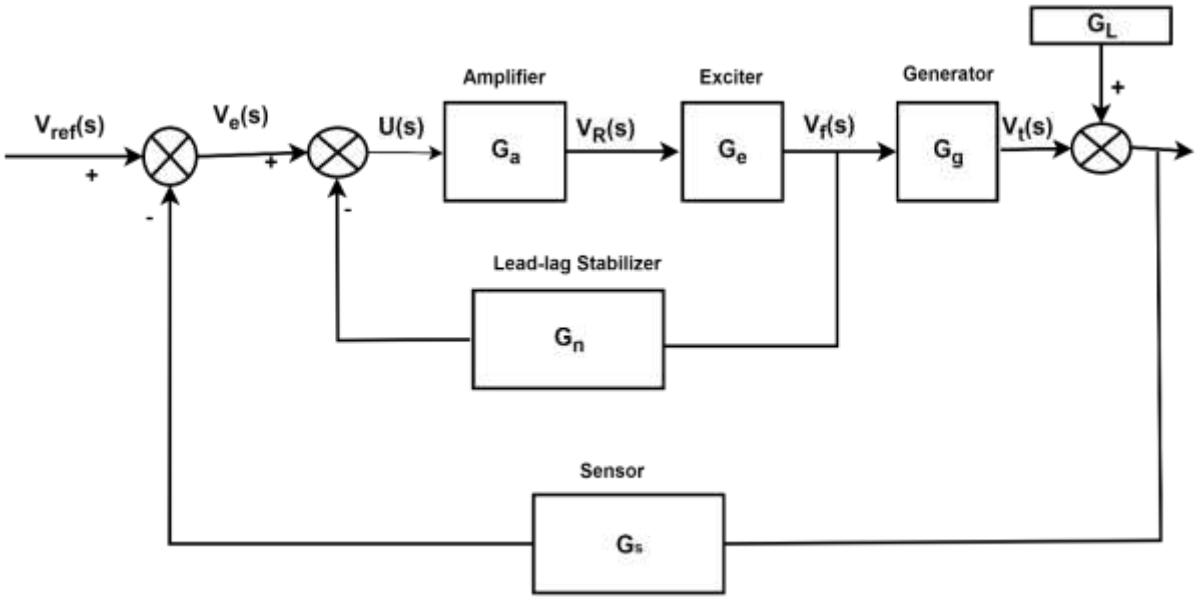

Figure 3. Compensated AVR Synchronous Generator System

Given the Lead-lag compensator and load in Figure 3, the system input, output, error signal, and control signal are $V_{ref}(s)$, $V_t(s)$, $V_e(s)$, and $U(s)$, respectively. The error signal from the first summing is given by equation (12), the control signal from the second summing is given by equation (13), and the forward path$V_R(s)z$, $V_f(s)$, and $V_t(s)$ are given as equation (14), (15), and (16), respectively.

$$V_e(s) = V_{ref}(s) - G_s V_t(s) \quad 12$$

$$U(s) = V_e(s) - G_n V_f \quad 13$$

$$V_R(s) = G_a U_s(s) \quad 14$$

$$V_f(s) = G_e V_R(s) \quad 15$$

$$V_t(s) = G_g V_f(s) - G_L(s) \quad 16$$

Substituting Eq. (12) into Eq. (15) resulted in Eq. (17). Substituting Eq. (17) into Eq. (16) and after simplifying and finding the common factors, the final expression is given as Eq. (18).

$$V_f(s) = G_a G_e \left(V_{ref}(s) - G_s V_t(s) - G_n V_f(s)\right) \quad 17$$

$$V_t(s) = \frac{G_a G_e G_g V_{ref}(s) - G_a G_e G_g G_n V_f(s) - G_L(s)}{1 + G_a G_e G_g G_s} \quad 18$$

Finding and substituting the expression for V_f given in Eq. (17) as Eq. (19), and also Eq. (19) into Eq. (18) to eliminateV_f, resulted in Eq. (20).

$$V_f(s) = \frac{G_e G_a (V_{ref}(s) - G_s V_t(s)}{1 + G_e G_a G_n} \quad 19$$

$$V_t(s) = \frac{G_a G_e G_g V_{ref}(s) - G_a G_e G_g G_n \left(\frac{G_e G_a (V_{ref}(s) - G_s V_t(s)}{1 + G_e G_a G_n}\right) - G_L(s)}{1 + G_a G_e G_g G_s} \quad 20$$

Let G_{CAVR} be the relationship between the V_t and the V_{ref}, the transfer function $G_{CAVR}(s)$ of the CAVR of the synchronous generator; therefore, the resulting closed-loop transfer function of the CAVR system is given as

equation (21), where parameters such as G_a, G_e, G_g, G_s, G_n and G_L are all represented in equations (2), (4), (6), (8), (10) and (11), respectively.

$$G_{CAVR}(s) = \frac{G_a G_e G_g (1+G_e G_a G_n)}{(1+G_a G_e G_g G_s)(1+G_a G_e G_n)+G_a^2 G_e^2 G_g G_n G_s} - \frac{G_L}{1+G_a G_e G_g G_s} \quad 21$$

2.3 Model-free adaptive control

The model-free adaptive control (MFAC) strategy is employed in the CAVR system to manage uncertainties and nonlinearities without a direct mathematical model of the system. MFAC real-time adaptation is applied to control actions based on input-output data; thus, it can manage complex, nonlinear systems like the AVR system. MFAC combines adaptive control and reinforcement learning principles for iterative system optimization [32]. The AVR system is a nonlinear system, and its dynamic equation can be represented by Eq. (22).

$$y(t+1) = f\left[y(t), y(t+1), \dots, y\left(t-n_y\right), u(t), u(t-1), \dots, u(t-n_u)\right] \quad 22$$

Where y(t) is the system output (V_t), u(t) is the control input (excitation voltage), n_y and n_u are the system orders, and finally f[·] is the unknown nonlinear function.

The dynamic system is simplified into a compact form of dynamic linearization using input-output variations given in Eq. (23).

$$\Delta y(t+1) = \phi(t)\Delta u(t) \quad 23$$

Where, $\phi(t)$ is the estimated iterative pseudo-gradient parameter, Equation (24) is the incremental change in output, and Equation (25) is the incremental change in input.

$$\Delta y(t+1) = y(t+1) - y(t) \quad 24$$

$$\Delta u(t) = u(t) - u(t-1) \quad 25$$

The pseudo-gradient $\phi(k)$ for parameter estimation is iteratively estimated as equation (26).

$$\hat{\phi}(t) = \hat{\phi}(t-1) + \eta\left(\frac{[\Delta y(t) - \hat{\phi}(t-1)\Delta u(t-1)]\Delta u(t-1)}{\mu + |\Delta u(t-1)|^2}\right) \quad 26$$

where η is the learning rate of the step size between $(0 < \eta \leq 2)$, μ is the small positive constant that prevents division by zero, and $\hat{\phi}(t)$ is the pseudo-gradient at step t.

The MFAC control law aims to minimize the performance criterion [33] given in Equation (27), whereas the optimal control increment is given in Equation (28).

$$J\big(u(t)\big) = |y_r(t+1) - y(t+1)|^2 + \lambda|\Delta u(t)|^2 \quad 27$$

$$\Delta u(t) = \frac{\rho\hat{\phi}(t)[y_r(t+1) - y(t)]}{\lambda + |\hat{\phi}(t)|^2} \quad 28$$

where, $y_r(t+1)$ is the desired reference voltage, λ is the weighing factor to trade off tracking accuracy and control effort, and ρ id the step factor of between $0 < \rho \leq 1$.

The control input u_{MFAC} is updated iteratively as equation (29), and a reset criterion is introduced to ensure stability and prevent divergence, as if equations (30) and (31) are true, then equation (32). The MFAC algorithm is given as Algorithm 1.

$$u_{MFAC}(t) = u_{MFAC}(t-1) + \Delta u(t) \quad 29$$

$$\left|\hat{\phi}(t)\right| \leq \in_N \quad 30$$

$$|\Delta u(t-1)| \leq \in_N \quad 31$$

$$\hat{\phi}(k) = sign(\hat{\phi}(t)) \in_N \quad 32$$

Where, $\in_N$ is the small threshold value required to maintain stability under noisy conditions.

Algorithm 1: MFAC algorithm

Set initial conditions:
$\hat{\varphi}(1)$: *initial value*
$u_{MFAC}(1)$: *initial control*
For $\boldsymbol{t \geq 1}$:
Step 1: *Calculate* $\Delta u(t-1)$ *and* $\Delta y(t)$
Step 2: *Update* $\hat{\varphi}(t)$ *using parameter estimation*

$$\hat{\phi}(t) = \hat{\phi}(t-1) + \eta\left(\frac{\left[\Delta y(t) - \hat{\phi}(t-1)\Delta u(t-1)\right]\Delta u(t-1)}{\mu + |\Delta u(t-1)|^2}\right)$$

Step 3: *Apply reset mechanism*
If
$|\hat{\phi}(t)| \leq \in$ *or* $|\Delta u(t-1)| \leq \in$ *is true*
*then*a reset
$\hat{\phi}(t) = sign(\hat{\phi}(t)) \in_N$
*Step*4: *Compute control increment* $\Delta u(t)$

$$\Delta u(t) = \frac{\rho\hat{\phi}(t)[y_r(t+1) - y(t)]}{\lambda + |\hat{\phi}(t)|^2}$$

5. *Update control input*
$u_{MFAC}(t) = u_{MFAC}(t-1) + \Delta u(t)$
6. *Check for Convergence*
if converged, proceed to end, else retun to step 1

End

2.4 H-infinity Controller

The H-infinity (H_∞) controller is designed to ensure the robust performance and stability [34] of the CAVR system under varying load conditions. The generalized plant G_{CAVR} is represented in a state-space form. The state equation is given as equation (33), the performance output as equation (34), and the measured output as equation (35).

$$\dot{x}(t) = Ax(t) + B_1 w(t) + B_2 u_{h_\infty}(t) \quad (33)$$

$$z(t) = C_1 x(t) + D_{11} w(t) + B_{12} u_{h_\infty}(t) \quad (34)$$

$$y(t) = C_2 x(t) + D_{21} w(t) + D_{22} u_{h_\infty}(t) \quad (35)$$

where A, B_1, B_2, C_1, C_2, D_{ij} are the state-space matrices derived from $G_{CAVR}(s)$, $x(t)$ is the state vector of the CAVR system, A is the system matrix, B_1 is the load disturbance input matrix, B_2 is the control input matrix, C_1 is the performance output matrix, C_2 is the measured output matrix, D_{11} is the direct disturbance-to-performance matrix, D_{12} is the direct control-to-performance, D_{21}, is the direct disturbance-to-measured matrix, and D_{22} is the direct control-to-measured matrix.

The H_∞ controller is represented in a standard configuration, as shown in Figure 4. Plant *P* has two inputs: the exogenous input *w*, which includes both reference signals *r* and disturbances *d*, and the manipulated variables *u*. The system also has two outputs: the error signal z, which is to be minimiped, and the measured variable *y*, which

is used to control the system [35]. The relationship between the system's outputs and inputs in Figure 4 can be expressed as equations (36) and (37), while the controller K(s) computes the control action $u_{h_\infty}(s)$ as equation (38).

$$\begin{bmatrix} z \\ y \end{bmatrix} = G_{CAVR}(s) \begin{bmatrix} w \\ u \end{bmatrix} \quad 36$$

$$\begin{bmatrix} z \\ y \end{bmatrix} = \begin{bmatrix} G_{CAVR_{11}} & G_{CAVR_{12}} \\ G_{CAVR_{21}} & G_{CAVR_{22}} \end{bmatrix} \begin{bmatrix} w \\ u \end{bmatrix} \quad 37$$

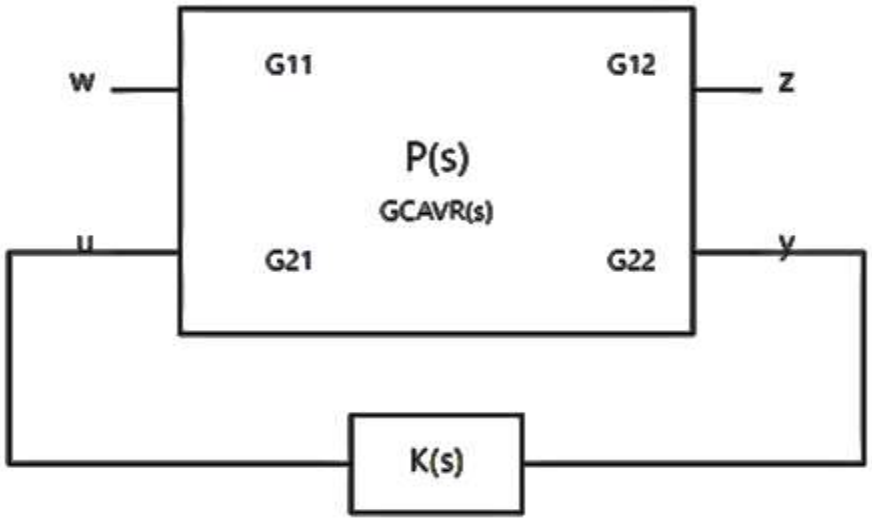

Figure 4. H-infinity Controller Block Diagram

$$u_{H_\infty}(s) = K(s)y(s) \quad 38$$

Where, G_{CAVR} is the CAVR transfer function, w is the exogenous inputs (r and d), r is the reference signals, d is the load disturbances.

The objective is to design K(s) that minimizes the H_∞ norm of the closed-loop transfer function$T_{zw}(s)$ such that the transfer function from exogenous inputs w to the error signals z satisfies the controller $K(s)$ condition in Eq. (39) under given performance constraints. The closed-loop relationship between z and w is given by the lower linear fractional transformation (LLFT) as equation (40), where, $F_\ell(G_{CAVR}, K)$ is given as equation (41).

$$||T_{zw}(s)||_\infty = sup\bar{\sigma}\big(T_{zw}(j\omega)\big) \leq \gamma \quad 39$$

$$T_{zw}(s) = F_\ell(G_{CAVR}, K) \quad 40$$

$$F_\ell(G_{CAVR}, K) = G_{CAVR_{11}} + G_{CAVR_{12}}K(I - G_{CAVR_{22}}K)^{-1}G_{CAVR_{21}} \quad 41$$

Where, F_ℓ is the lower linear fractional transformation, $\bar{\sigma}$ is the maximum singular value of the matrix of T_{zw}, $\gamma > 0$ is the performance bound, and $T_{zw}(s)$ closed-loop transfer function of the system from w to z.

The weighting function is incorporated to shape the system's performance and ensure trade-offs between tracking accuracy, disturbance rejection, and control effort [36]. The sensitivity weight W_1 in equation (42) minimizes the tracking error, the complementary sensitivity weight W_2 in equation (43) suppresses the load variation effect, and the control input weight W_3 in equation (44) limits the excessive control effort. Therefore, the weighted plant $G_W(s)$ is constructed by augmenting the original $G_{CAVR}(s)$ withW_1, W_2, and W_3 functions to incorporate the performance criteria to the original plant and expressed as equation (45), while the resulting augmentation is given as equation (46).

$$W_1(s) = \frac{s+\omega_b}{M(s+\omega_a)} \quad 42$$

$$W_2(s) = \frac{M(s+\omega_a)}{s+\omega_b} \quad 43$$

$$W_3(s) = \frac{s+\omega_c}{\in} \quad 44$$

$$G_W(s) = \begin{bmatrix} W_1(s) & 0 \\ 0 & W_2(s) \end{bmatrix} \begin{bmatrix} G_{CAVR_{11}}(s) & G_{CAVR_{12}}(s) \\ G_{CAVR_{21}}(s) & G_{CAVR_{22}}(s) \end{bmatrix} \begin{bmatrix} I & 0 \\ 0 & W_3(s) \end{bmatrix} \quad 45$$

$$G_W(s) = \begin{bmatrix} W_1(s)G_{CAVR_{11}}(s) & W_1 G_{CAVR_{12}}(s) W_3(s) \\ W_2 G_{CAVR_{21}}(s) & W_2(s) G_{CAVR_{22}}(s) W_3(s) \end{bmatrix} \quad 46$$

Where ω_aa ω_b and ω_c are the controlled frequency response, $\in$ is the small value that ensures that the control effort remains within acceptable limits, $M > 1$: desired maximum sensitivity.

The controller synthesis problem is formulated as an LMI optimization problem, and a positive definite matrix is introduced to ensure stability. The condition that ensures the stability of the system is given in equation (47), and the constraints are incorporated into the LMI framework to ensure the performance objectives are met, resulting in equation (48).

$$A'X + XA + B_2K + K'B_2' < 0 \quad 47$$

$$\begin{bmatrix} A'X + XA + B_2K + K'B_2' & XB_1 & C_1' \\ B_1' & -\gamma I & D_{11}' \\ C_1 & D_{11} & -\gamma I \end{bmatrix} < 0 \quad 48$$

Where W_1 sensitivity weight used to minimize the tracking error, W_2 is the complementary sensitivity weight used to shape the response of the system to disturbances, and W_3 is the control input weight used to limit the control effort, I represents the identity matrix, and $X > 0$ is the positive definite matrix.

The state-space representation of the controller is given by Equation (49) and (50).

$$\dot{x_\infty}(t) = Px_\infty(t) + Qy(t) \quad 49$$

$$u_{h_\infty}(t) = Rx_\infty(t) + Ty(t) \quad 50$$

where P, Q, R, and T are controller matrices obtained from the LMI, $x_\infty(t)$ is the state vector of the controller, $y(t)$ is the plant's measured output, and $u(t)$ is the plant's input.

The simulation results were analyzed to assess the controller's ability to regulate the generator's output voltage under various load conditions.

$$t_p = \frac{\pi}{\omega_d} \quad 51$$

$$t_r = \frac{\pi-\phi}{\omega_n} \quad 52$$

$$t_s = \frac{4}{\zeta\omega_n} \quad 53$$

$$M_p = Exp - \frac{\zeta\pi}{\sqrt{1-\zeta^2}} \times 100\% \quad 54$$

where t_p is the peak time, t_r is the rise time, t_s is the settling time, M_p is the percentage overshoot, ω_d is the damped natural frequency of the system, ϕ is the phase angle (radians), ζ is the damping ratio, and ω_n is the underdamped natural frequency.

3. RESULTS AND DISCUSSION

The performance of the two employed H-infinity and MFAC control schemes in regulating the terminal voltage of the synchronous generator through the AVR system was investigated by investigating the performance of the controllers under four load conditions (no-controller, 20% load, 50% load, and 80% load) under four controlling situations (compensated-controller, and with controllers-H-infinity and MFAC). Moreover, the performance validation is examined by comparing the performance of the H-infinity controller, MFAC, No-controller, and Compensated-No-controller situations against each other to determine the best strategy under the four loading conditions. The AVR, and the controllers and the Lead-lag compensation parameters are shown in Tables 2 and 3, respectively, and the MATLAB/SIMULINK R2023a software was used for the implementation. The time vector for the simulation was initially 100 s but was later reduced to 60 s to improve the visibility of the graphs. The desired voltage was 220 V.

Table 2. AVR System Component Parameters

Component	Amplifier		Exciter		Generator		Sensor	
	K_a	T_a	K_e	T_e	K_g	T_g	K_s	T_s
Value	27	0.07	4.5	0.72	1.00	0.00	1.34	0.002

Table 3. Controllers' Parameters

Parameters	T_{n1}	T_{n2}	α	η	ρ	λ	$\in_N$	γ	W_1	W_2	W_3	ϵ	M
	0.65	0.34	1.87	0.11	0.93	0.06	0.02	2.4	0.21	0.34	1.6	0.002	80

3.1 No-Controller Situation

The response of the system in the absence of any controller shows that the terminal voltage of the synchronous generator exhibits significant deviations from the desired voltage of 220 V as the load increases. For instance, the terminal voltage remains at the desired level (220 V) under no-load conditions, indicating that the system is stable without any external disturbances. However, as the load increases to 20%, 50%, and 80%, the terminal voltage begins to drop to 208, 190, and 172 V, respectively, as shown in Figure 5 and Table 4. This demonstrates the AVR system's inherent inability to maintain voltage regulation under dynamic load conditions without a control mechanism. The results highlight the need for a control strategy to mitigate voltage deviations, especially under higher load conditions.

Table 4. No-controller Condition

Load Condition	K_L	T_L (s)	Control Strategy	Terminal voltage (V)	Control Strategy	Terminal voltage (V)
No-load	0	0		220.0		220.0
20% Load	0.2	30	No-controller	208.0	No-controller with lead lag	210.4
50% Load	0.5	30		190.0		196.0
80% Load	0.8	30		172.0		181.6

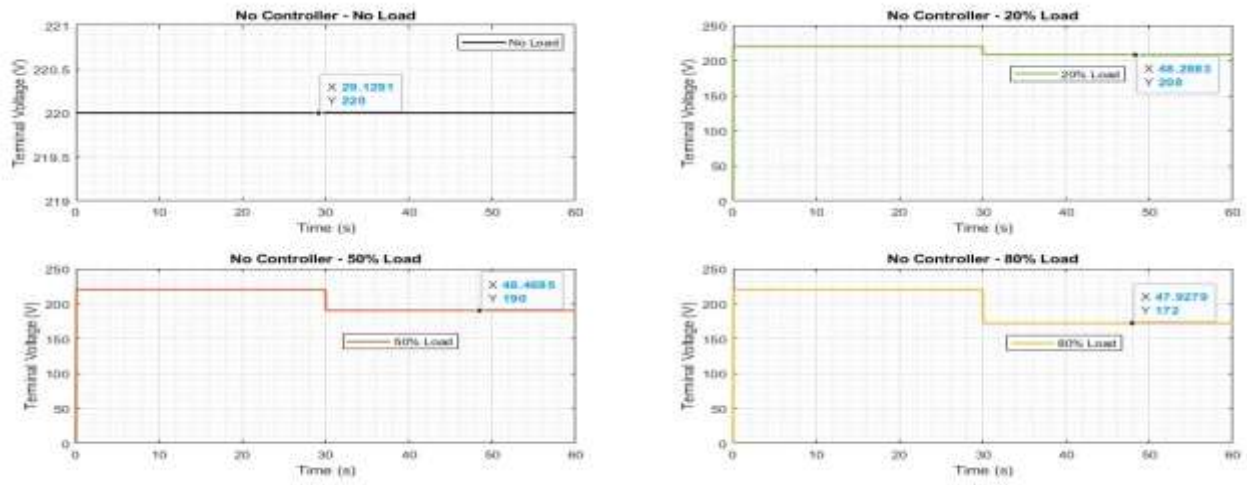

Figure 5. Terminal Voltage in the All-load No-controller Situation

3.2 No-Controller with Lead-Lag Compensation

A stabilizer is also attached to the AVR system to compensate for the deviation in the terminal voltage by introducing a lead-lag compensation, which improves the voltage regulation compared to the no-controller situation. The terminal voltage remains at 220 V under no-load conditions, similar to the no-controller case. However, with 20%, 50%, and 80% load conditions, the terminal voltage improved from no-controller voltage deviations of 208, 190, and 172 V to 210.4, 196, and 181.6 V, respectively, as shown in Figure 6 and Table 4. Although the Lead-lag compensation provides some improvement, the terminal voltage still significantly deviates from the desired value, particularly under higher loads. This indicates that while Lead-lag compensation can enhance system performance and reduce the steady-state error, it is insufficient to achieve robust voltage regulation across all load conditions.

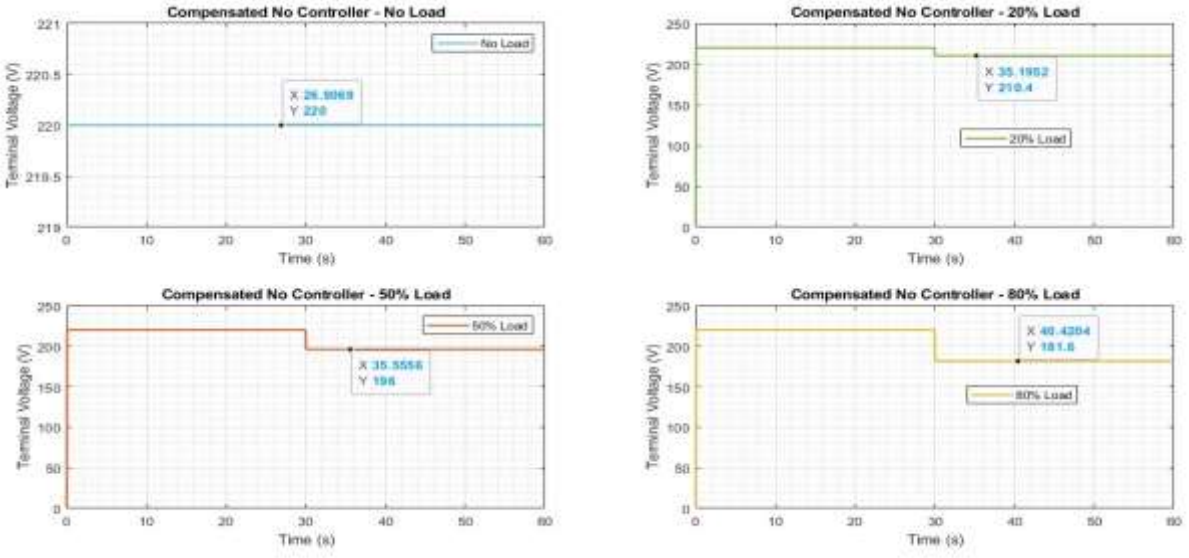

Figure 6. Terminal Voltage in the All-load Compensator No-controller Situation

3.3 MFAC Controller Situation

The MFAC is then implemented into the CAVR system. The control strategy demonstrates a significant improvement in voltage regulation compared to both the No-controller and the No-load controller with lead-lag compensation scenarios. Under no-load conditions, MFAC achieves a rise time of 0.36 s, a settling time of 0.42 s, and a percentage overshoot of 40.14%, as shown in Figure 7 and Table 5. Although the overshoot is relatively high, the system quickly stabilizes. Under 20%, 50%, and 80% load conditions, the rise time and settling time increased, but the percentage overshoot decreased to 2.19%, 5.47%, and 8.76%, respectively (Figures 8, 9, and 10). The (a) part of the aforementioned Figures denotes the full response over time, while the (b) part shows the load-side response from the load time of 30 s to provide a clearer picture of the load impacts. This indicates that the MFAC controller effectively reduces voltage deviations under load variations, although it takes more time to settle with higher loads. Notably, the settling times for the 20%, 50%, and 80% load conditions are 30.33, 30.39, and 30.45 s, respectively, corresponding to actual settling times of 0.33, 0.39, and 0.45 s after the load impact at 30 s. This demonstrates the controller's ability to quickly stabilize the system after a load disturbance. Figure 11 shows the performance comparison of the MFAC strategy under different load conditions.

Table 5. MFAC performance under various load conditions

Load Condition	K_L	T_L (s)	Control Strategy	Rise time (s)	Settling time (s)	Percentage Overshoot (%)
No-load	0	0		0.36	0.42	40.14
20% Load	0.2	30	MFAC	0.00	0.33	2.19
50% Load	0.5	30		0.12	0.39	5.47
80% Load	0.8	30		0.24	0.45	8.76

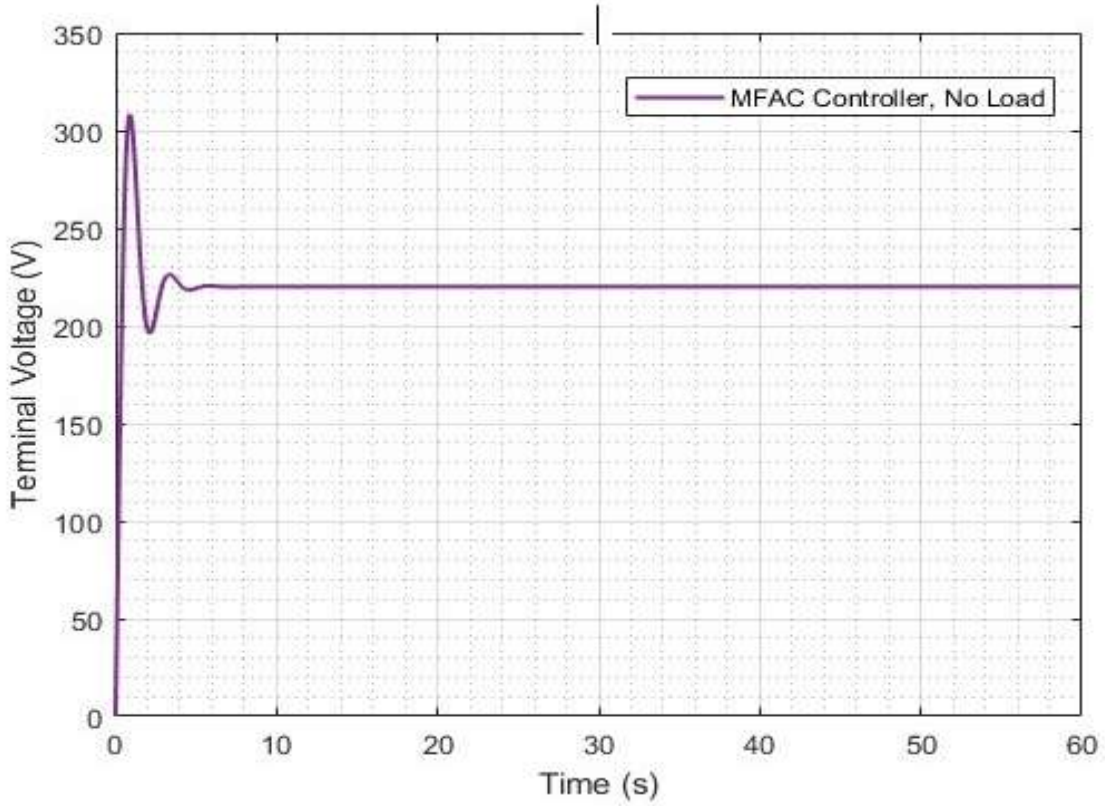

Figure 7. Terminal Voltage with MFAC in the No-load Condition

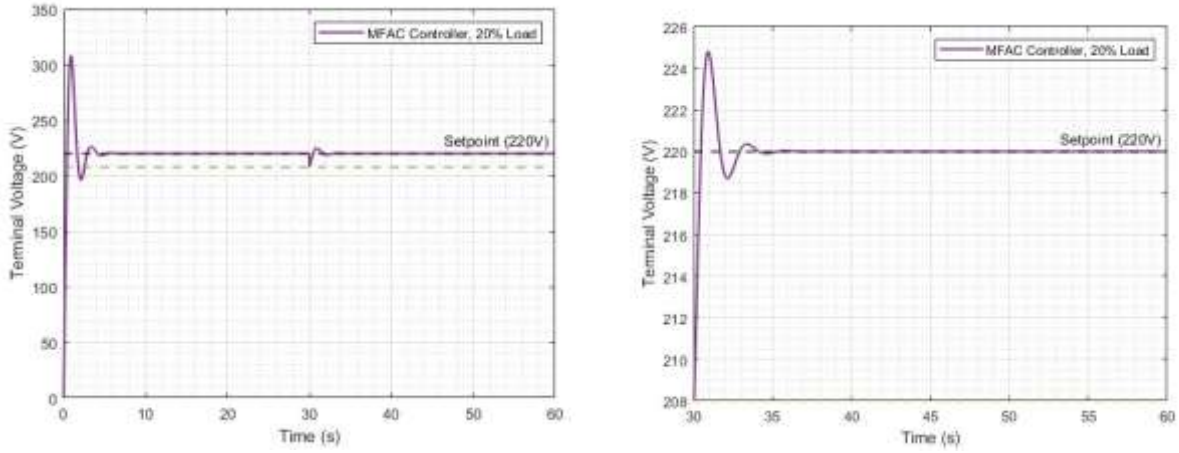

(a) Full (b) Load Side (t = 30)

Figure 8. Terminal Voltage with MFAC at 20% load

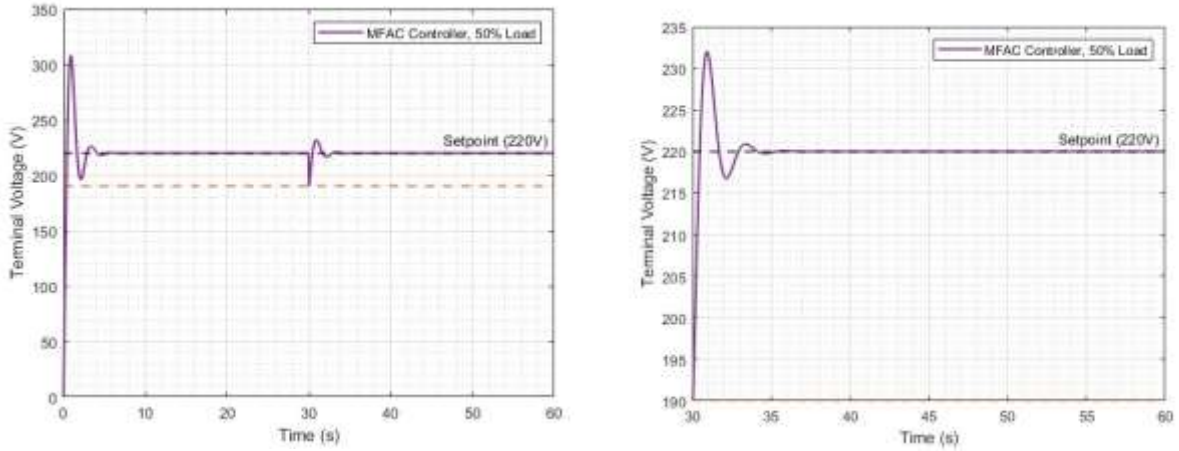

(a) Full (b) Load Side (t = 30)

Figure 9. Terminal voltage with MFAC at 50% load

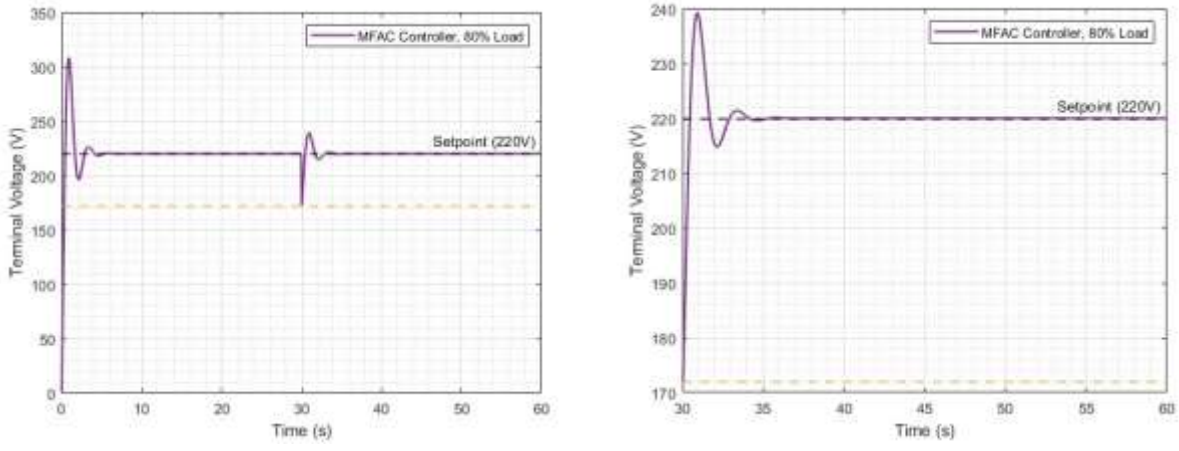

(a) Full (b) Load Side (t = 30)

Figure 10. Terminal Voltage with MFAC at 80% load

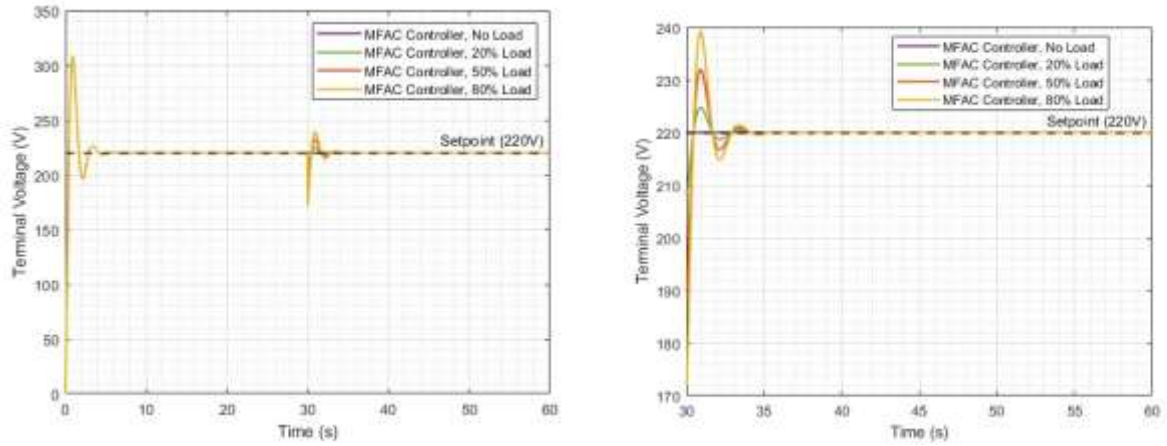

(a) Full (b) Load Side (t = 30)

Figure 11. Comparative Terminal Voltage with MFAC under All-load Conditions

3.4 H-infinity controller situation

The introduction of the H-infinity controller shows that it outperforms the MFAC in terms of both voltage regulation and dynamic response. Under no-load conditions, the H-infinity controller exhibited a rise time of 1.56 s, a settling time of 1.98 s, and a percentage overshoot of 17.15% (Figure 12). Although it takes a longer time (not significantly) to settle compared to the MFAC controller, the overshoot is significantly lower. Under 20%, 50%, and 80% load conditions, the H-infinity controller achieves minimal overshoot of 0.78%, 1.95%, and 3.12%, respectively, and maintains stable voltage regulation. The settling time increases slightly with higher loads, but the overall performance remains robust, demonstrating the superior capability of the H-infinity controller in handling load variations, as shown in Figures 13, 14, and 15. Figure 16 compares the performance under different load conditions. For instance, the settling time for the 20%, 50%, and 80% load conditions correspond to actual settling times of 0.87, 0.47, and 0.65 s, respectively, after the load impact at 30 s. This further underscores the ability of the H-infinity controller to quickly stabilize the system after a load disturbance. The metrics are shown in Table 6.

Table 6. H-infinity controller performance under various load conditions

Load Condition	K_L	T_L (s)	Control Strategy	Rise time (s)	Settling time (s)	Percentage Overshoot (%)
No-load	0	0	H-infinity Controller	1.56	1.98	17.15
20% Load	0.2	30		0.00	0.87	0.78
50% Load	0.5	30		0.18	1.47	1.95
80% Load	0.8	30		0.66	1.65	3.12

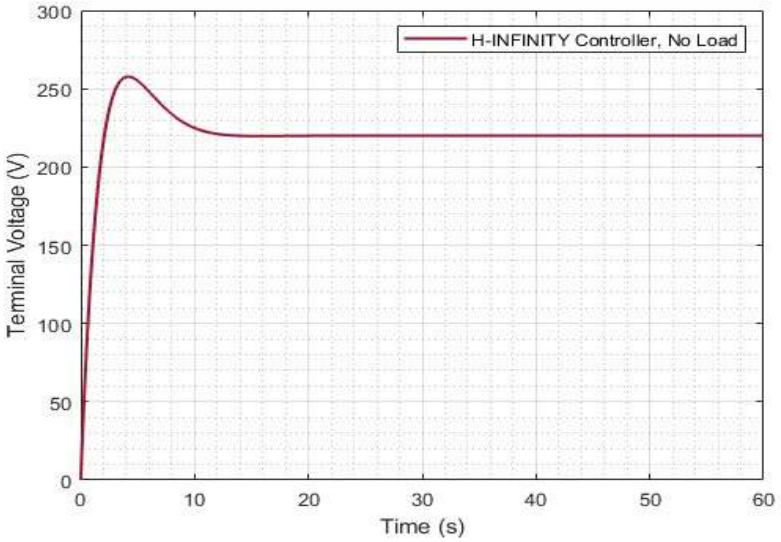

Figure 12. Terminal Voltage with H-infinity controller under No-load Condition

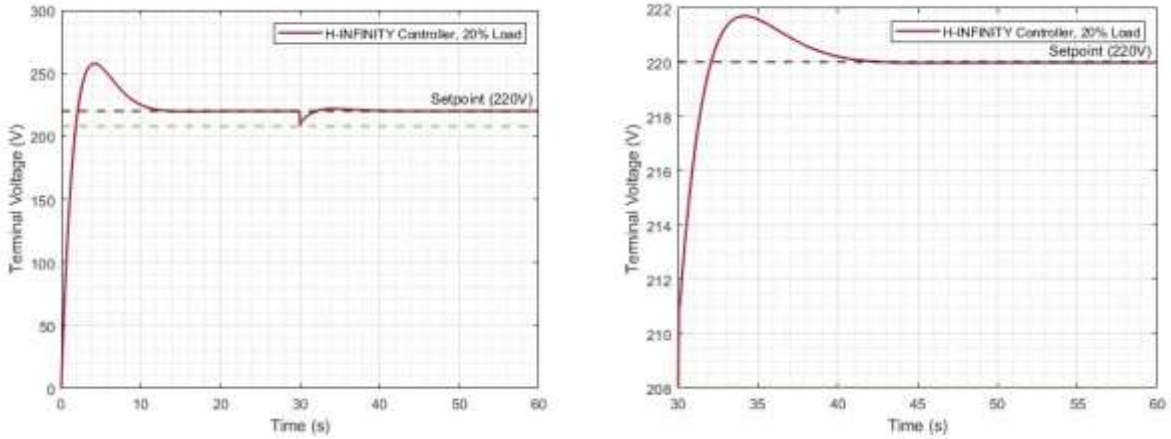

(a) Full (b) Load Side (t = 30)

Figure 13. Terminal Voltage with H-infinity controller at 20% load

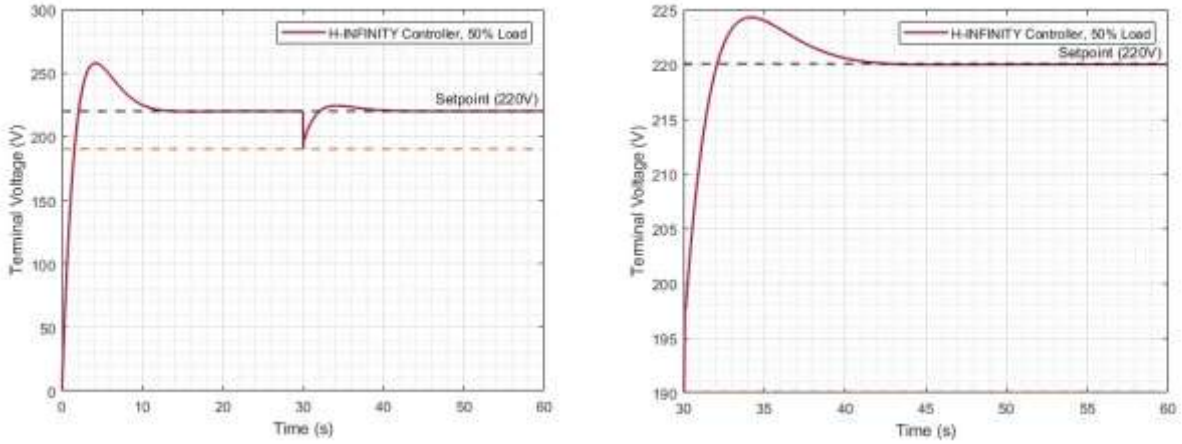

(a) Full (b) Load Side (t = 30)

Figure 14. Terminal Voltage with H-infinity controller at 50% load

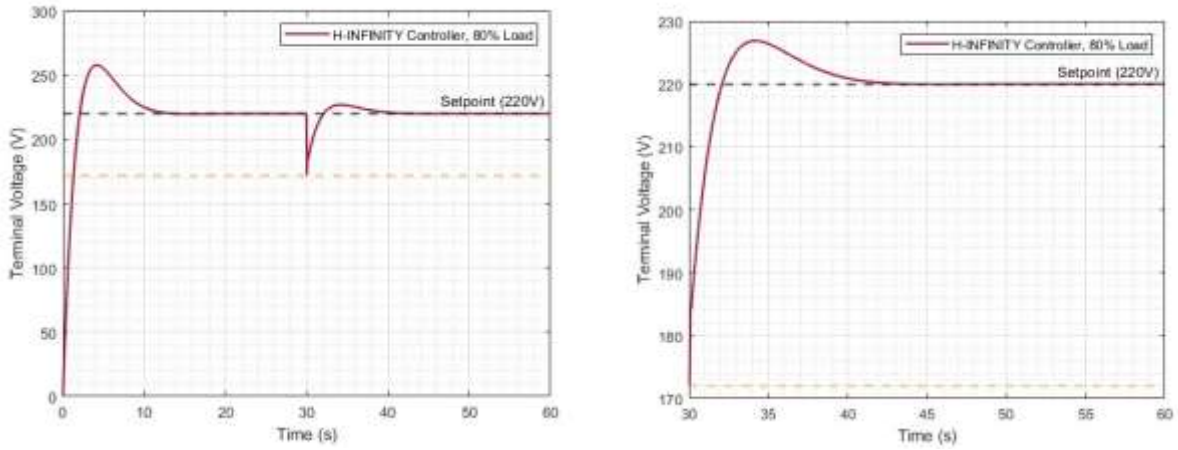

(a) Full (b) Load Side (t = 30)

Figure 15. Terminal Voltage with H-infinity controller at 80% load

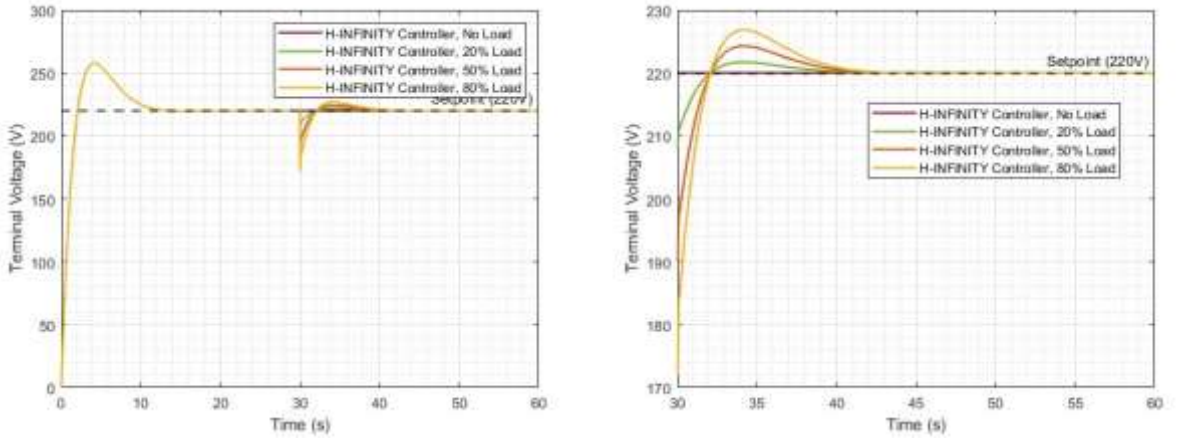

(a) Full (b) Load Side (t = 30)

Figure 16. Comparative Terminal Voltage with H-infinity controller under All-load Conditions

3.5 MFAC and H-infinity

To compare the performances of the two employed control strategies, the MFAC controller demonstrates a faster dynamic response with a shorter rise and also settles quickly across all load conditions, making it suitable for applications where quick voltage regulation is required. However, it exhibits a higher percentage overshoot (40.14%), particularly under no-load (Figure 17) and heavy load (8.76%) conditions, which may compromise stability. In contrast, the H-infinity controller provides superior stability, with significantly lower overshoot of 0.78% at 20% load in Figure 18 and 3.12% at 80% load in Figure 20, albeit with slightly longer rise and settling times, though not much significant. Therefore, the MFAC controller excels in speed, and the H-infinity controller offers better robustness and precision, making it the preferred choice for applications demanding reliable voltage regulation under varying load conditions.

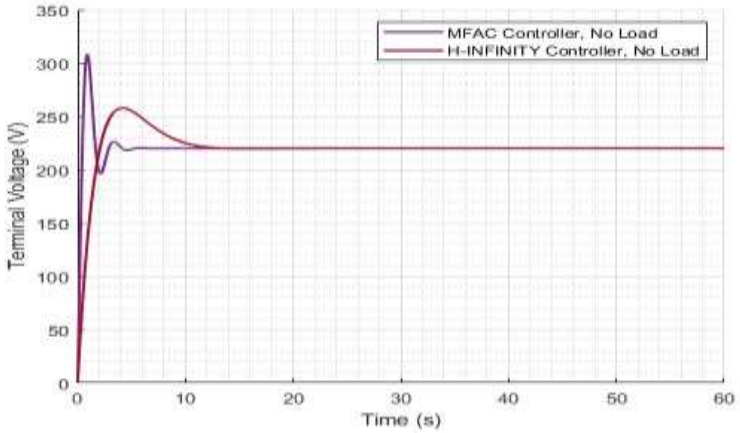

Figure 17. Comparison of the Terminal Voltage between MFAC and H-infinity controller at No-load Condition

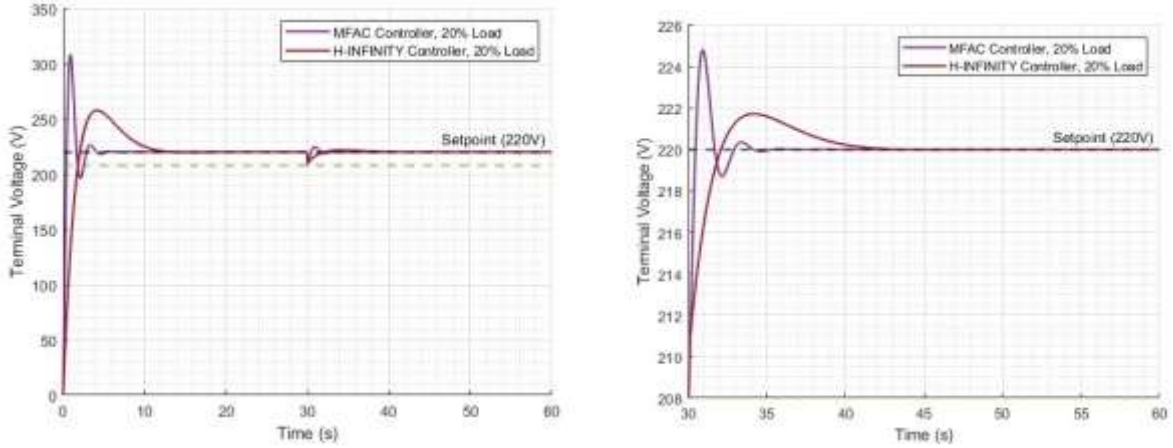

(a) Full (b) Load Side (t = 30)

Figure 18. Terminal Voltage Comparison between MFAC and H-infinity controller at 20% load

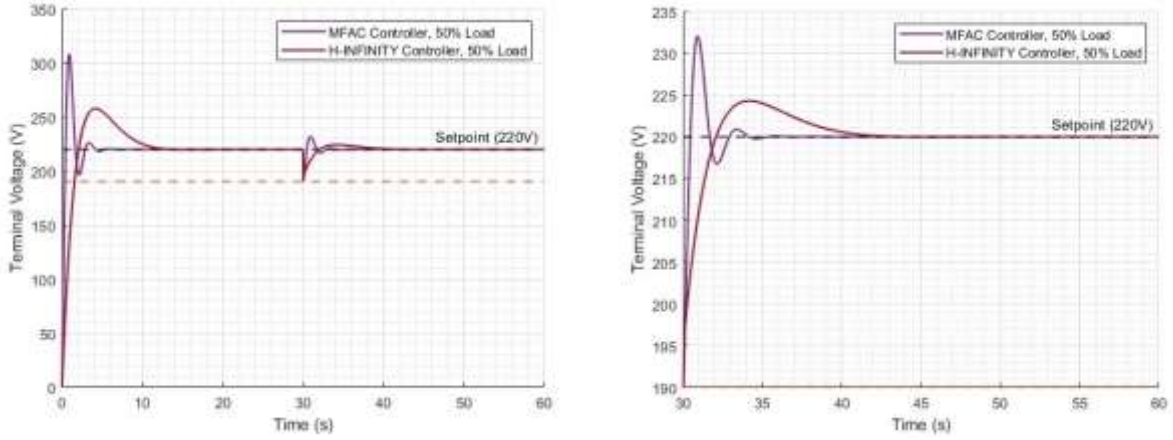

(a) Full (b) Load Side (t = 30)

Figure 19. Comparison of the terminal voltage between MFAC and H-infinity controller at 50% load

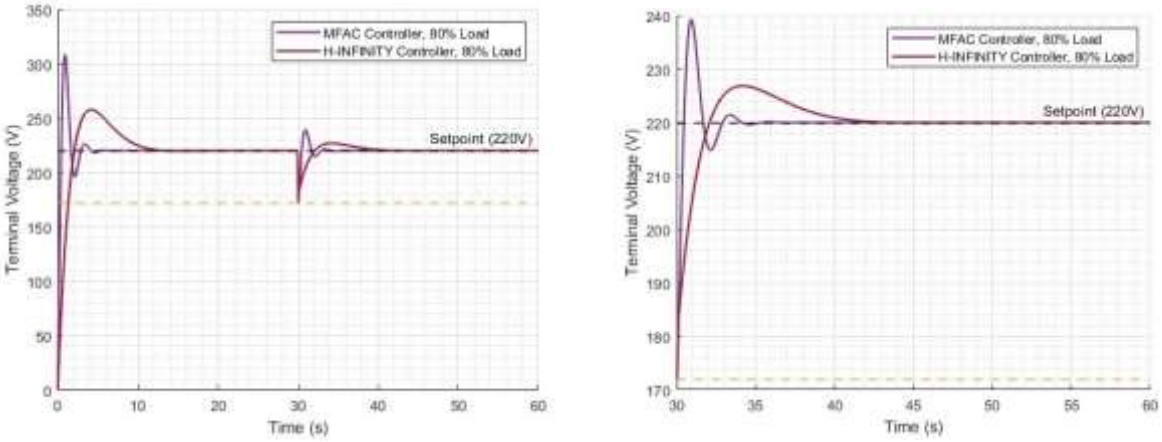

(a) Full (b) Load Side (t = 30)

Figure 20. Terminal Voltage Comparison between MFAC and H-infinity controller at 80% load

4. RESULTS ANALYSIS

The results in Tables 4, 5, and 6 show that the H-infinity controller provides the best overall performance in terms of voltage regulation and dynamic response under varying load conditions. The No-controller case does not exhibit voltage stability with respect to load variations, and the use of lead-lag compensation as a stabilizer yields only marginal improvements. The MFAC controller performs satisfactorily but with increased overshoot and extended settling time compared to the H-infinity controller. The H-infinity controller, on the other hand, exhibits the least overshoot and demonstrates stable voltage regulation under all load conditions; therefore, it offers the best control approach.

These results indicate that the ability of the H-infinity controller to provide stable voltage regulation under varying loads makes it a good candidate for real-world applications in power systems with load oscillations. These results emphasize the significance of selecting a control strategy based on system-specific requirements and expected load conditions.

5. CONCLUSION

A comparative study of MFAC and H-infinity controllers for AVR systems provides significant results for power system stability. Compared with the no-controller, which has huge voltage fluctuations (dropping to 172 V at 80% load) and leadslag compensation offers only marginal improvement, advanced control methods have a significant advantage. The fast response of MFAC (settling within 0.42 s at no-load) is offset by its huge overshoot (40.14%), limiting its reliability. The H-infinity controller outperforms alternatives with excellent stability (0.78% overshoot at 20% load) and stable operation in all test cases. The results verify the feasibility of the H-infinity controller in real power systems subject to dynamic load fluctuation. Future research is recommended to study hybrid control schemes of the two controllers to further enhance system performance. This paper provides a valuable reference for power engineers who seek to enhance grid stability using state-of-the-art voltage regulation techniques.

REFERENCE

A. T. Humod, A. S. Abdulsada, Study of AVR control of synchronous generator based on intelligent technique, University of Technology, Electrical and Electronic Engineering Department, Baghdad, Iraq, 2011.

Shadoul, M., Ahshan, R., Al-Abri, R. S., Al-Badi, A., Albadi, M., Jamil, M. A. (2022). Comprehensive review on a virtual-synchronous generator: topologies, control orders and techniques, energy storages, and applications. Energies, 15 (2022) 22, pp. 8406. DOI: 10.3390/en15228406.

Pasala, G., Pinni, S., Varma, C., Naga, S., Kalyan, C., Ravikumar, V., Srinivasulu, A., Bhimsingh, B., Rajesh, A., Mohd-Nadhir, A., & Sathish, K. (2023). Dynamic behavior and stability analysis of automatic voltage regulator with parameter uncertainty. International Transactions on Electrical Energy Systems, 2023, pp. 6662355. DOI: 10.1155/2023/6662355.

Hassan, R., Javid, Z., Shah, A., & Ahmed, R. (2019). Impact of load variations on power system performance under high penetration of wind generation, 2019, pp. 166-171.

Hosseinzadeh N, Aziz A, Mahmud MA, Gargoom A, Rabbani M. Voltage stability of power systems with renewable-energy inverter-based generators: a review. Electronics. 2021; 10:1151. DOI: 10.3390/electronics100201151.

Mazibuko, N., Akindeji, K. T., & Sharma, G. (2022). Modeling and performance analysis of an automatic voltage regulator (AVR) using model predictive controller (MPC). Proceedings of the IEEE PES/IAS PowerAfrica, 2022, pp. 1-5.

M. Rawat, S. Vadhera, Voltage stability assessment techniques for modern power systems, Handbook of Research on Smart Power System Operation and Control, 10 (2020), pp. 40. https://doi.org/10.1016/j.smartpower.2020.10.10

J. Ritonja, B. Polajžer, Analysis of synchronous generators' local mode eigenvalues in modern power systems, Appl. Sci. 12 (2021) 195. DOI: 10.3390/app12010195.

Omar, A., Marei, M., & Attia, M. A. (2023). Comparative study of AVR control systems considering a novel optimized PID-based model reference fractional adaptive controller. Energies, 16 (2023) 2, pp. 12. DOI: 10.3390/en16020812.

Mojumder, R. H., Roy, N. K., 2021. PID, LQR, and LQG controllers to maintain the stability of an AVR system at varied model parameters, Military Institute of Science and Technology (MIST), Dhaka-1216, Bangladesh, 2021.

Takialddin, A. S., Osman, A., & Khalid, A. A. (2018). Overview of model free adaptive control technology. IAES International Journal of Artificial Intelligence, 7 (2018) 4, pp. 165-169.

D. R. Alene, U. Somarajan, Structured H-Infinity controller for an uncertain deregulated power system, Int. J. Control Theor. Appl. 10 (2018) 6, pp. 425-433.

Anantwar, H., Lakshmikantha, B. R., & Sundar, S. (2019). Optimized controller design using an adaptive bacterial foraging algorithm for voltage control and reactive power management in off-grid hybrid power system. International Journal of Image, Graphics and Signal Processing, 1 (2019), pp. 33-43.

A. Sivanandhan, G. Thriveni, Optimal design of controller for automatic voltage regulator performance enhancement: a survey, Electr. Eng., 2024. DOI: 10.1007/s00202-023-02196-5

Can, C., Andic, C., Ekinci, S., & Izci, D. (2023). Enhancing transient response performance of automatic voltage regulator system by using a novel control design strategy. Electrical Engineering, 2023, pp. 105.

Muoghalu, C. N., Uju, I. U., & Mbachu, C. B. (2020). Performance response improvement of automatic voltage regulator using linear quadratic Gaussian tuned controller. International Journal of Latest Technology in Engineering, Management & Applied Science, 9 (2020) 11, pp. 6-12.

P. Govindan, Evolutionary algorithms-based tuning of PID controller for an AVR system, Int. J. Electr. Comput. Eng. 10 (2020), pp. 3047-3056.

Micev, M., Calasan, M., Ali, Z. M., Hasanien, H. M., & Aleen-Abdel, S. H. E. (2020). Optimal design of automatic voltage regulation controller using hybrid simulated annealing - Manta ray foraging optimization algorithm. Ain Shams Engineering Journal, 2 (2020), pp. 1-17.

E. Çelik, R. Durgut, Performance enhancement of automatic voltage regulator by modified cost function and symbiotic organisms search algorithm, Eng. Sci. Technol., 21 (2018). DOI: 10.1016/j.jestch.2018.08.006.

Sajnekar, D. M., Kolhe, M. L., Deshpande, S. B., Moharil, R. M., Patidari, N. P., & Ogura, N. (2018). Design of PID controller for automatic voltage regulator and validation using hardware in the loop technique. International Journal of Smart Grid and Clean Energy, 7 (2018), pp. 75-89.

Eswaramma K, Kalyan GS (2017) An automatic voltage regulator (AVR) system control using a PI-DD controller, International Journal of Advance Engineering and Research Development, 4 (2017), pp. 499-506.

Mittal, M. K., & Rai, P. (2016). Performance analysis of conventional controllers for automatic voltage regulator (AVR). International Journal of Latest Trends in Engineering and Technology, 7 (2016), pp. 338-344.

S. Ekinci, B. Hekimoğlu, Improved kidney-inspired algorithm approach for tuning of PID controller in AVR system, IEEE Access 7 (2019), pp. 39935-39947. DOI: 10.1109/ACCESS.2019.2906960.

J. K. Nøland, S. Nuzzo, A. Tessarolo, E. Alves, Excitation system technologies for wound-field synchronous machines: survey of solutions and evolving trends. IEEE Access, 7 (2019), pp. 109699-109718. DOI: 10.1109/ACCESS.2019.2934119.

Gopi, P., Reddy, S. V., Bajaj, Z., Zaitsev, L., & Prokopz, L. (2024). Performance and robustness analysis of V-Tiger PID controller for automatic voltage regulator. Sci. Reps, 14 (2024), pp. 7867. DOI: 10.1038/s41598-024-58477-x.

IEEE, IEEE guide for synchronous generator modeling practices and parameter verification with applications in power system stability analyses, IEEE Std 1110-2019, 100 (2020) 2, pp. 1-92.

S. Tsegaye, K. Fante, Analysis of synchronous machine excitation systems: comparative study, Energy and Power Engineering, 10 (2018), pp. 1492-1496.

Eze, P. G., & Uebari, B. (2021). Control techniques for enhancing the performance of automatic voltage regulator in power system stability, Multidisciplinary International Journal of Research and Development, 1 (2021) 1, pp. 82-94.

Alawad, N. A., Rahaman, N. G., 2019. Particle swarm optimization with Pade approximation based-model reduction of automatic voltage regulation, International Journal of Latest Engineering Science, 2 (2019) 5, pp. 1-5.

Y. Zaw, W. Yu, Performance analysis of automatic voltage regulator in power generation system, Int. J. Sci. Eng. Appl. 8 (2019), pp. 180-185.

Movahedi, A., Halvaei, A., & Gharehpetian, G. B. (2019). LVRT improvement and transient stability enhancement of power systems based on renewable energy resources using coordination of SSSC and PSSs controllers. IET Renewable Power Generation, 13 (2019).

Y. Wang, C. Shen, J. Huang, H. Chen, Model-free adaptive control for unmanned surface vessels: a literature review, Syst. Sci. Control Eng. 12 (2024) 1. DOI: 10.1080/21642583.2024.2316170

Z. Chen, P. Ju, Z. Wang, D. Huang, L. Shi, K. Deng, Research on multi-objective control of PPCI diesel engine combustion process based on data driven modeling, Energy and AI, 2025, pp. 100472. https://doi.org/10.1016/j.energyai.2025.07.0472. DOI: 10.1016/j.egyai.2025.100472

Lu K, Feng G, Ding B. Robust H-Infinity tracking control for a valve-controlled hydraulic motor system with uncertain parameters in the complex load environment. Sensors. 2023; 23:9092. DOI: 10.3390/s23229092

Hidalgo, H., Orosco, R., Huerta, H., Vázquez, N., Hernández, C., & Pinto, S. (2023). A high-voltage-gain DC-DC boost converter with zero-ripple input current for renewable applications. Energies, 16 (2023) 13, pp. 4860. DOI: 10.3390/en16134860

M. Dulau, S.-E. Oltean, The effects of weighting functions on the performances of robust control systems, Proc. 63 (2020) 1, 46. DOI: 10.3390/proceedings2020063046